2.6. NaDodSO$_4$–PAGE

Samples from spicule extracts containing 1–3 μg of protein were dissolved in loading buffer (Roti-Load, Roth, Karlsruhe, Germany), boiled for 5 min, and then subjected to 10% polyacrylamide gel electrophoresis, containing 0.1% sodium dodecyl sulphate (NaDodSO$_4$–PAGE; Laemmli, 1970). After separation, the gels were washed in 10% methanol (supplemented with 7% acetic acid) for 30 min and then stained in Coomassie Brilliant blue as described (Müller et al., 2005). In parallel, silver staining was performed according to the described procedure (Radojkovic and Kusić, 2000).

2.7. Determination of proteolytic activity

Spicule extracts from *Monorhaphis* were obtained avoiding HF (see above) and assayed for cathepsin L-activity as described (Dvorak et al., 2005). The soluble protein fraction was added to the reaction assay (0.2 ml volume) as described (Quian et al., 1989; Mort, 2002) in 96-well plates (Nunc 96 MicrowellTM Plates) at room temperature. The assay contained 10 μM Z-Phe-Arg-AMC as substrate and incubation was performed for 60 min at room temperature. A standard curve was established with 7-amino-4-methylcoumarin (AMC); the fluorescence of the free AMC released was determined using an excitation at 355 nm and an emission at 460 nm in an F-2000 Hitachi fluorescence spectrophotometer. The activity was calculated and given in nmoles AMC released/mg protein × min (Dvorak et al., 2005). Five parallel experiments were performed, and the means and standard deviations were calculated (Sachs, 1984).

Where here indicated the *Monorhaphis* extracts were preincubated (30 min; 20 °C) with 1 μM E-64.

2.8. Binding studies with biotinylated E-64

Biotinylated E-64 was obtained from unlabeled E-64 by coupling the inhibitor via amine–PEO$_2$–Biotin (Pierce, Rockford, IL, USA) and using the cross linker 1-ethyl-3-[3-dimethylaminopropyl]carbodiimide (EDC), according to the instructions of the manufacturer (Pierce). This labeled E-64 was used as a probe to detect the enzymatically active center. *Monorhaphis* extract (10 μl), obtained by solubilization with a 50-mM Tris–HCl buffer (pH; 8.5; 10% (v/v) glycerol), was supplemented with 10 μl of 50 mM Na-acetate buffer (pH 5.5; 100 mM NaCl, 1 mM EDTA). After an activation period of 10 min at room temperature 5 μl (50 μM final concentration) of biotinylated E-64 was added to the activated enzyme and the mixture was incubated at 22 °C for 1 h. This sample was mixed with 5 μl of 6 × Laemmli sample buffer and heated for 5 min at 95 °C. The samples were analyzed by NaDodSO$_4$–PAGE (10% gels) according to Laemmli (1970). Then the proteins were transferred to a PVDF membrane. The biotin-[E-64] protein complex was visualized using the biotin/avidin VECTASTAIN Elite ABC detection system (Hsu et al., 1981; Vector Labs., Burlingame, CA, USA). The signals were enhanced by the chemiluminescence procedure using the "western horse radish peroxidase substrate"/Luminol Reagent (Millipore, Schwalbach, Germany).

2.9. Mechanical property measurement

The measurement for the flexural properties of an individual, giant basal spicule samples (between 30 and 35 mm in length) were tested as described (Levi et al., 1989; Sarikaya et al., 2001; Autumn et al., 2006). The samples were cut from the spicule using a disk saw, to avoid cracking. The spicule sample was fixed in a 3-point bending system (WDW 3020, Changchun; China), selecting a fixture with a 20-mm span and an articulated center loading rod at a crosshead rate of 0.2 mm/min. The diameters of the tested spicules ranged from 2.1 to 2.6 mm. Tests were performed with a computer-controlled MTS servo-hydraulic test frame. Crosshead displacement and load were automatically recorded throughout the tests. For these studies freshly collected giant basal spicules were used, which had remained in wet conditions (in seawater) until their use for the experiments.

2.10. Analytical method

For the quantification of protein the Bradford method (Compton and Jones, 1985; Roti-Quant solution—Roth) was used.

3. Results

Primarily two hexactinellid species have so far been analyzed to understand the biophysical, biomechanical and biochemical processes of spicule formation, *Euplectella aspergillum* (Fig. 1A) and *Monorhaphis chuni*/*Monorhaphis intermedia* (Fig. 1B–D). In the present study we used the giant basal spicules, and—where indicated—comitalia from *Monorhaphis*, for the analysis.

3.1. Growth of the giant basal spicules: axial cylinder and lamellar sheet

One *Monorhaphis* specimen grows around one giant basal spicule (Fig. 1B). The soft body is arranged in an ellipsoid growth form axially along the spicule, and has ≈5 cm large osculi along the major axis. The giant basal spicule is fixed asymmetrically within the body and is closer to the osculi than to the opposite pore-rich part of the body (Fig. 1B and D). While the giant basal spicule fixes the complete soft body to the ground, several comitalia are usually associated with one oscular section. Already in 1904, Schulze described the lamellar organization of the spicules from *Monorhaphis*, focusing on the giant basal spicules. In the center of the spicule lies the axial cylinder which appears to be less foliated; this cylinder surrounds

the axial canal which harbors the axial filament (Fig. 1C). Operationally, the spicules can be divided into three sections; the axial canal, the axial cylinder and the lamellar zone.

The lamellar thickening growth and especially the longitudinal growth of the spicules can be conveniently analyzed using the comitalia. The immature spicules have open tips that are not covered by siliceous material and expose their axial filaments (Fig. 2A). The diameter of the axial filament within the rectangular axial canal measures 2–5 μm. Only few comitalia spicules are sealed by silica at their tips (Fig. 2B), suggesting that these are mature and terminally grown spicules. In contrast, to the comitalia the giant basal spicules have a thinner axial canal of only 2 μm or less (Fig. 2C). The axial canal is surrounded by a 150–200 μm thick axial cylinder which appears—in contrast to the peripherally located lamellar zone—not distinctly structured into lamellae (Fig. 2C). If the giant basal spicules are broken the central cylinder remains almost intact, while the peripheral lamellar zone undergoes fracturing into concentric piles of chipped lamellae (Fig. 2D). At higher magnification of the peripheral lamellar zone it can be seen that the individual silica layers (comprising microcracks), which are between 3 and 8 μm thick are separated from each other by small (0.1–0.2 μm) interlamellar gaps (Fig. 2E). If slightly etched lamellae are inspected it becomes obvious that they are traversed by small non-siliceous canals, which are distinctly displaced between adjacent lamellae (Fig. 2E). The fractured surface of the spicule shows an unbroken axial cylinder and a series of fractured lamellae (Fig. 2F). The sites of fractures are staggered between the lamellae.

The zonation in (i) the outer lamellar zone, (ii) the axial cylinder and (iii) the central axial canal can be distinguished not only in the giant basal spicules (Fig. 2C), but also in the comitalia (Fig. 3A). After etching of the fracture surface it becomes obvious that the axial cylinder displays likewise lamella-like structures which are interspersed by cavities formed during the dissolution process (Fig. 3C and D). In the center of the spicule the rectangular axial

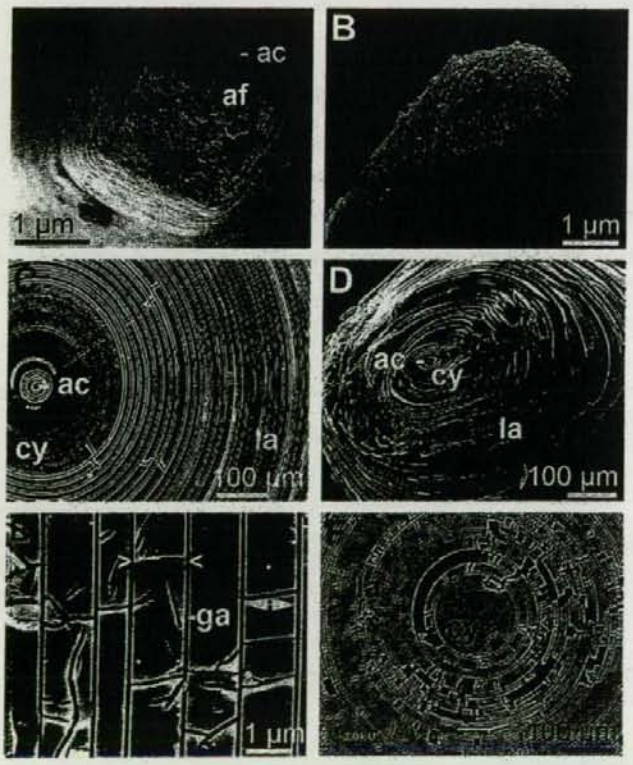

Fig. 2. Morphology of the giant basal spicule/comitalia from *Monorhaphis*, SEM analyses. (A and B) Growing comitalia spicules. During axial growth, the spicules show at their tips an open axial canal (ac), which discloses the axial filament (af). (B) In a terminal stage the tips are covered with silica. (C–F) Giant basal spicules. (C) A cross-section shows the zonation of the spicules: axial canal (ac); axial cylinder (cy); lamellar peripheral zone (la). (D) A broken spicule, showing the more massive axial cylinder (cy) with the axial canal (ac) and the piles of the peripheral lamellae (la). (E) At a higher magnification the silica lamellae become exposed. The lamellae (↔) are interspersed with small non-siliceous canals (> <), and are separated from each other by gaps (ga). (F) A fractured spicule was cut and inspected. It becomes apparent that the fractured lamellae (la) have microcracks which are displaced. In the center of the spicule is the axial cylinder (cy). The scale bars are included.

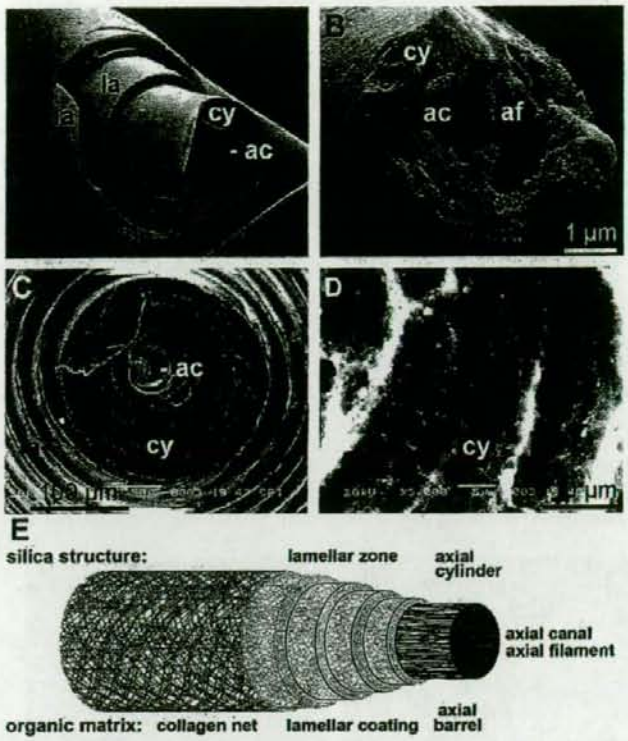

Fig. 3. Zonation within the spicules; SEM analyses of comitalia (A and B) and giant basal spicule (C and D). (A) The three morphological zones within the spicules: central axial canal (ac), axial cylinder (cy), lamellar, peripheral zone (la) can be clearly distinguished in a growing comitalia. (B) A broken tip of a comitalia with the axial cylinder (cy), the axial canal (ac) and the axial filament (af). (C and D) Fracture surface of a giant basal spicule. After etching, lamellar structures appear within the axial cylinder. In addition, canal-like perforations in the siliceous material are seen. (E) Scheme summarizing the three morphological zones. The silica structures (with their organic components); the axial canal (axial filament), the axial cylinder (axial barrel) and the lamellar zone (lamellar coating). The surface of the spicule is surrounded by a collagen net.

canal with the axial filament is located (Fig. 3B). A schematic view of a spicule is given in Fig. 3E, highlighting the surface collagen net, followed inwards by the lamellar zone (with its organic component, the lamellar coating) and the axial cylinder (axial barrel).

3.2. Collagen layer around the spicules and its silicification

The surface of a spicule is covered by a loosely attached collagen net (Fig. 4A). In a previous study (Müller et al., 2007a) the diameter of the collagen fibers, forming this net, has been determined to be 25 nm. The net is interspersed with circular to oval holes of 7–15 µm in diameter. Especially towards the tip of the spicule an increased silicification of the collagen fibers can be assumed, according the SEM images (Fig. 4B–F). In the initial stage of this silicification process, individual collagen fibers can be distinguished which are occasionally covered with irregular deposits (Fig. 4B–D). Later, the individual deposits fuse and start to pile up cover sheets/patches carrying on their surfaces also irregular deposits (Fig. 4E and F).

3.3. Silicification at the collagen sheet: SEM/EDX analyses

EDX analysis was applied to identify the elemental composition of the deposits on the collagen net. The region analyzed was documented by SEM imaging (Fig. 5A). The EDX determination revealed that the irregular deposits, which have been identified on the collagen fibers, are of siliceous deposits; since major EDX signals are seen which correspond to carbon (C), oxygen (O) and silicon (Si) Fig. 5B. The respective peaks (K_α) of silicon and oxygen in the spectrum are due to silica. The presence of a carbon peak is indicative of the protein matrix. EDX also shows the presence of gold which is due to the sputtering of the sample with gold.

3.4. Stepwise dissolution of the giant basal spicule with HF: lamellar coating and axial barrel

For these experiments, loosely attached organic material was removed from the comitalia by utrasonication. A distinction between the axial cylinder and the surrounding

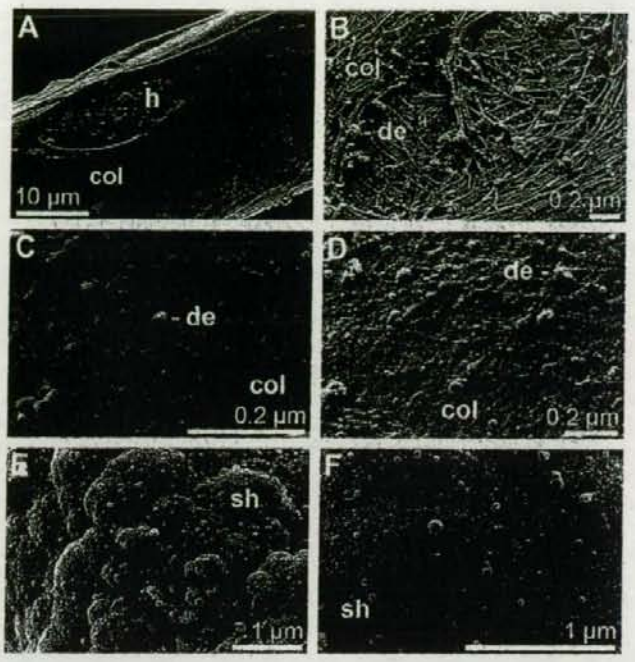

Fig. 4. Loosely attached collagen layer (col) around the spicules; SEM analyses (A–D). (A) The collagen net, perforated with holes (h), surrounds the spicules. (B–D) Individual collagen fibers (col) are shown which are decorated with irregular deposits (de). (E and F) Continuous cover sheets/patches (sh) on the surface of the collagen net, suggesting a silicification process.

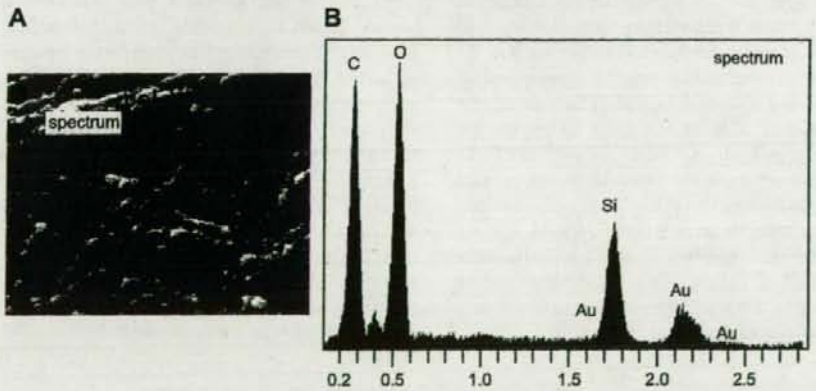

Fig. 5. Particles deposited onto the collagen net and surrounding the spicule were analyzed by SEM/EDX. (A) The collagen layer (col) with its individual fibers is shown; SEM analysis. One region had been selected for EDX analysis (spectrum). (B) After EDX analysis, primarily carbon (C), oxygen (O) and silicon (Si) signals were found. In addition, gold signals (Au) can be identified which originate from the sputtering of the sample with gold.

lamellar zone is possible even by light microscopic inspection, using Nomarsky DIC imaging (Fig. 6A and B). The axial cylinder occupies about half of the diameter of the comitalia, usually 150 µm.

The spicules were subjected to HF dissolution; after about 1 min of exposure to HF the lamellar zone starts to dissolve. The dissolution starts from the cracks of the spicule, primarily following the gaps between the lamellae thus forming saw-tooth edges (Fig. 6C). During this process the lamellar zone can be distinguished from the axial cylinder by the protruding ends of dissolving individual lamellae. Finally, after an exposure time of 30 min, the

intact axial cylinder remains (Fig. 6D). The dissolution of the axial cylinder proceeds from the periphery on without revealing individual lamellae. The siliceous material in the axial cylinder is completely dissolved after 90 min (Fig. 6G).

By application of different dyes, the proteinaceous components in the two zones surrounding the axial canal can be visualized. Addition of Coomassie Brilliant blue to the HF solution results in an immediate staining of the proteins released from the lamellar zone (Fig. 6E). During the initial phase of dissolution a proteinaceous coating (lamellar coating) becomes uncovered which only remains transiently intact (Fig. 6E) until the organized sheets disintegrate to irregular clumps/aggregates (Fig. 6F). Prior to this disintegration, the lamellar coating blisters. The second tubing is formed from proteins of the axial cylinder. This structure is termed here axial barrel (Fig. 6G). In contrast, to the lamellar coating the axial barrel is composed of individual rope-like filaments (Fig. 6G–J). These structures can be stained besides by Coomassie Brilliant blue also with Sirius Red; the latter stain does not color proteins from the lamellar zone or from the axial canal (Fig. 6G and I). In addition, the axial barrel is stained with the fluorescent dye Rhodamine 123 (Fig. 6H). The existence of the rope-like structures in the axial cylinder can be visualized even in an unstained state, applying Nomarsky DIC optics (Fig. 6J).

3.5. Analysis of the proteinaceous lamellar coating

Two procedures were used to isolate the proteinaceous lamellar coating: (i) limited dissolution with HF and (ii) gentle extraction of lamellae with an HF-free buffer. As outlined in the previous section, the lamellar zone is readily dissolved by HF during a 30-min period. The subsequent zone, the axial cylinder, releases the axial barrel during an additional 60-min period. A closer inspection of the organic material released from the lamellar zone revealed initially a fibrous, net-like meshwork, which still has contact to the siliceous lamellar layers (Fig. 7A), as can be visualized with Coomassie Brilliant blue. These structures also can be seen by SEM optics (Fig. 7B). As outlined in the previous paragraph, the meshwork collapses and forms the irregular clumps/aggregates (Fig. 7C and D).

In a parallel series, the siliceous lamellae were mechanically removed from the axial cylinder and then used for the extraction under nondenaturing condition with a Tris-based lysis-buffer (pH 7.5), as outlined under "Methods". The isolated lamellae are shown in Fig. 7E; if those siliceous sheets were subjected to Coomassie Brilliant blue they were only slightly stained (Fig. 7F). This result was taken as an indication that the bulk of the protein does not exist on the silica surface or between the lamellae.

To substantiate this conclusion we tried to identify the proteinaceous component in the siliceous lamellae *in situ*, by application of the high-resolution SEM technique. For these studies siliceous lamellae were only exposed for a short period to HF (5 min). The images revealed that the stacked lamellae lost most of their siliceous components and exposed their proteinaceous matrix (Fig. 7G and H). The siliceous surfaces of the lamellae remained and are supported by palisade-like pillar structures, to be interpreted as proteinaceous material; the individual pillars have a diameter of 0.1–0.2 μm and a length of 5–10 μm (Fig. 7H). Hence, these pillars traverse the previously silica-filled lamella. Since for the high resolution SEM analyses broken spicules, which had not been polished with emery paper, have been used we see no reason to assume that these pillar structures are artificial.

The proteinaceous material, obtained by these two methods, was characterized by $NaDodSO_4$–PAGE (Fig. 8A). The matrix protein released by partial dissolution of the spicules with HF (15 min) was found to be almost completely insoluble in a buffer lacking a chaotropic agent, or β-mercaptoethanol. If the sediment was dissolved in the PAGE sample buffer, supplemented with $NaDodSO_4$ and β-mecaptoethanol, one distinct protein could be identified with an apparent size of 27 kDa (Fig. 8A lane b). Consequently the sediment was treated with 6 M urea, supplemented with 10% (v/v) β-mercaptoethanol, for 30 min at 60 °C. This solution dissolved the sediment completely and one single component, a 27-kDa protein, could be identified by $NaDodSO_4$–PAGE (Fig. 8A lane c). In parallel, the protein was extracted from the lamellae in the Tris-based lysis-buffer (pH 7.5), and analyzed by $NaDodSO_4$–PAGE. Again, only one protein species of a size of 27 kDa was found (not shown). Staining of the gels with silver resulted in the same protein pattern (data not shown).

Fig. 6. Stepwise dissolution of the silica shell around the axial filament of the spicule (comitalia) by treatment with HF solution, as described under "Materials and methods"; light microscopic analysis. (A and B) Initial phase, in the absence of HF. Already based on different light refraction (Nomarsky DIC imaging) the three zones within the spicule can be distinguished; the axial canal (ac), the axial cylinder (cy) and the lamellar zone (la). (C) Initial phase of the dissolution; solubilization of the lamellar zone (la) starts after 1–3 min. (D) After complete dissolution of the lamellar zone (treatment for 30 min) the axial cylinder (cy) which surrounds the axial canal/axial filament (af) is exposed. (E) The lamellar coating (lac), which is released from the lamellar zone after 8 min, surrounds the axial cylinder (cy), and becomes stained with Coomassie Brilliant blue. (F) After an HF treatment for 8–15 min this proteinaceous coating (lac) ruptures and disintegrates into irregular clumps/aggregates. Inside of them, a second proteinaceous axial barrel (axb) is released from the axial cylinder, that becomes likewise stained with Coomassie Brilliant blue. This barrel originated from the axial cylinder (cy). (G) The axial barrel (axb), completely freed of silica after an HF-treatment of 90 min, can be stained positive with Sirius Red. Inside of this structure the axial filament (af) can be identified, which is not stained by Sirius Red. (H) The axial barrel (axb) and the axial filament (af) become brightly stained with the fluorescence dye Rhodamine 123. (I) Higher magnification of the axial barrel (axb). (J) The individual unstained ropes of the axial barrel (axb) can be distinguished by Nomarsky DIC imaging. All size bars: 20 μm.

3.6. Determination of the proteinase active site with labeled E-64

The protein extract from the lamellae was analyzed for enzymatic, proteolytic activity, using the cathepsin L substrate Z-Phe-Arg-AMC, as described under Section 2. Under those conditions a proteolytic activity of the *Monorhaphis* extract was determined with 278 ± 49 nmol AMC released/mg × min. This sample could be inhibited with E-64; 1 μM of this inhibitor reduced

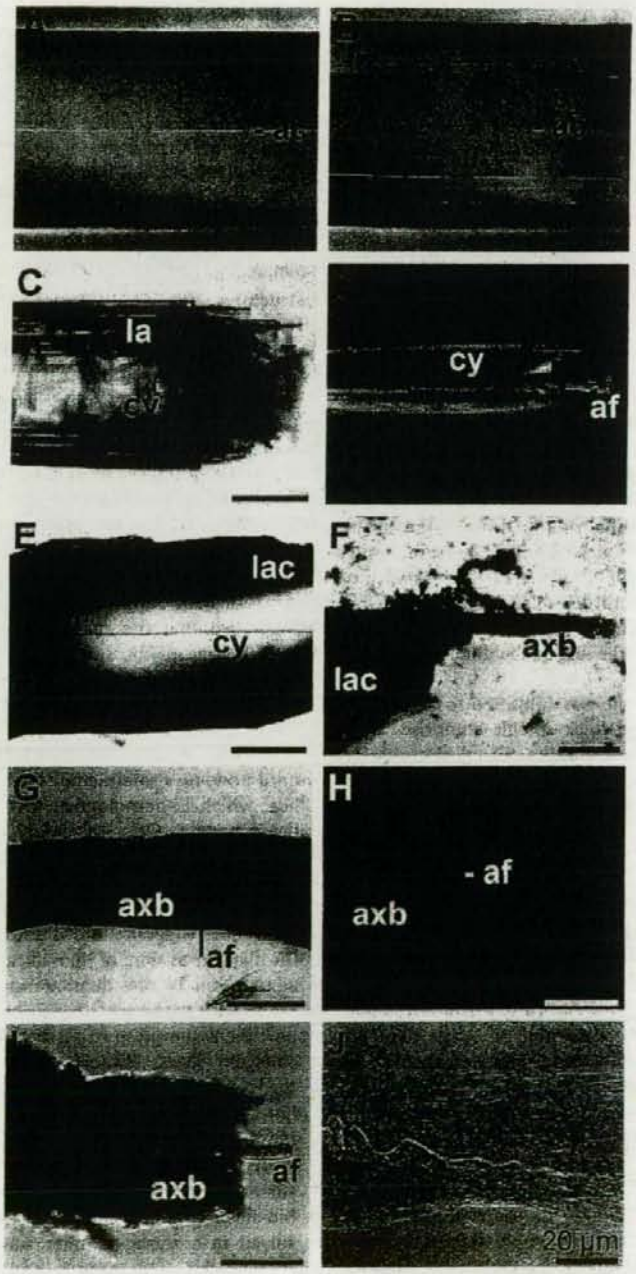

the activity by over 90% (21 ± 16 nmol AMC/mg protein × min).

In the next series biotin-labeled E-64 was used as a probe to identify the protease on the blot. The lamellar protein extract was size separated, the proteins were blot-transferred and the protein(s) which had been bound to biotinylated E-64 was visualized. The resulting blot showed one labeled molecule of an apparent size of 27 kDa (Fig. 8B lane a). If the protein(s) was first incubated with a surplus of unlabeled E-64 (20 μM) and subsequently incubated with biotinylated E-64, no band could be observed after blotting (Fig. 8B lane b). These results were taken as indication that the lamellar extract contains proteolytic activity.

3.7. Mechanical stability of the giant basal spicules

A sample from an unbroken spicule was subjected to a classical bend test (Fig. 9C). The representative load-displacement curve showed several characteristic points which we explain as follows (Fig. 9B). The linear increase A–B reflects the elastic response of the outer layers of the spicule; at point B (230 N) the first fiber crack occurs. The deflection B–C does not drop to zero but is fixed according to the viscoelastic view (Mayer et al., 2005) (and/or due to breaking of lamellar packets) by the more central lamellar layers at 115 N. The increment of the load until the second cracking event reaches a value of 150 N at D; the subsequent displacement of the curve reaches the same value as that after the first crack (115 N) at E; the elasticity of the spicule reaches 130 N until the third crack at F occurs. Subsequently, a broad range of load is recorded G–H which reflects the random cracking of the different lamellae within the axial cylinder.

A partially cracked spicule was subjected to SEM analysis (Fig. 9A). The 2.2-mm thick spicule comprises three fracture sites, which are marked in Fig. 9A; all those cracks traverse several lamellae. In the center of the spicule the axial cylinder shows no distinct linear fracture zone.

4. Discussion

The explanation of growth and forms in multicellular organisms is a prime challenge for a developmental biologist, especially regarding the understanding of formation of rigid bio-organic material, e.g. skeletal elements. Also in sponges growth forms are genetically controlled (Müller, 2005); these animals are composed of only relatively loosely attached cells, which—nevertheless—share all basic characters with cells found in higher metazoan phyla (Müller et al., 2004). Only recently, the question for the morphogenetic formation of the different forms of the spicules has been addressed both in Demospongiae (Müller et al., 2004; Wiens et al., 2006) and in Hexactinellida (Aizenberg et al., 2005; Müller, 2005). It is not yet understood, which proteins determine in these animals the sophisticated construction of the spicules. Collagen is surely one organic extracellular matrix constituent that is intimately connected with spicule growth and shape (Eckert et al., 2006; Ehrlich and Worch, 2007); the collagen net might act as an envelope in which the spicules develop (Schröder et al., 2006). In hexactinellid sponge spicules, the axial filament within the axial canal is thin, around 1–2 μm, compared with the dimensions of the spicules, which can reach sizes of 3 m in length and 6–8 mm in diameter (Aizenberg et al., 2004, 2005; Müller et al., 2007a; Wang et al., 2007). It could be shown that in demosponges (Müller et al., 2005; Schröder et al., 2006) and in hexactinellids (Aizenberg et al., 2005) growth of spicules proceeds by appositional deposition of concentric silica layers around the axial canal/axial filament.

In the present study we focused on the sectorial arrangement/composition of the organic components within the morphological regions of the spicules, the axial cylinder and the lamellar zone using the largest bio-silica structures, the giant basal spicules from *Monorhaphis*. Based on microscopic inspection these spicules, like the comitalia from the same organisms, could be divided into (i) the central, axial canal, (ii) the subsequent inner axial cylinder and (iii) the outer lamellar zone, composed of well distinct concentrically arranged silica lamellae. Cross sections suggested that the axial cylinder is more solid, compared to the peripheral lamellae. Limited etching with HF of cross sections discloses that the axial cylinder is not as homogenous, but comprises furrowed cavities of sizes between 0.1 and 2 μm in diameter. Since the diameter of the axial cylinder in these giant basal spicules remains largely constant, approximately 150–200 μm, it might be concluded that the outer lamellar zone is the principal growth zone of the spicules. There the 50–500 individual silica lamellae are piled up appositionally, resulting in a variation of the diameter of the spicules from 0.2 to 8 mm.

Focusing on the organic composition of the spicules, until now, no protein could be identified yet in hexactinellids, which is homologous to the silicateins known from demosponges. Only the related enzyme cathepsin L has been identified in this sponge class (Müller et al., 2007b). The outer surface of the *Monorhaphis* spicules is surrounded by a collagen fiber net. Electron microscopic inspection suggests that these fibers function as matrix for the deposition of bio-silica. EDX studies prove this assumption by the demonstration that silicon is present in this area together with oxygen. These results do not support the assumption of Ehrlich and Worch (2007) that it is collagen itself, which catalyzes bio-silica formation throughout the spicules. The collagen net is perforated by holes of constant sizes of 7–15 μm, which could act (during the process of the lamellar thickening growth of the spicules) like an expansion tube. Inwards, the collagen net surrounds the lamellar zone. Stepwise digestion of the bio-silica with HF revealed that the lamellar zone is dissolved in a zigzag manner, starting at the gaps between the lamellae. This process had been described already by

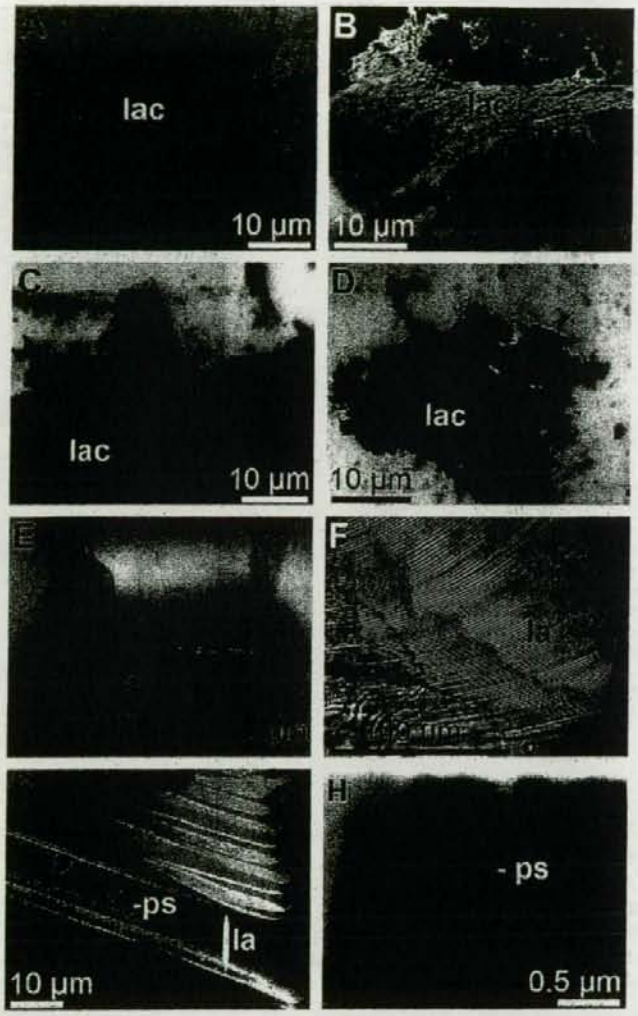

Fig. 7. Protein release from the lamellar zone (lamellar coating (lac)). (A–D) Stepwise release of the protein from the lamellar zone by limited dissolution of spicules with HF. Protein, net-like meshwork, was released during a 15-min HF treatment and stained during dissolution with Coomassie Brilliant blue (A) or the sample was immediately subjected to SEM analysis (B). After a longer exposure (30 min) the released protein was stained with Coomassie Brilliant blue and resulted in an aggregation to irregular clumps (C and D). In one series, lamellae were mechanically separated (E) from the axial cylinder. A sample of separated lamellae (la) treated with Coomassie Brilliant blue (0.1%, w/v) and inspected by light microscopy (F). (G and H) Almost completely dissolved silica material from lamellae of the peripheral zone of the spicules was analyzed by SEM (high-resolution imaging). At a lower magnification (G) one lamella with its proteinaceous structures is shown; the borders of one lamella (la) are marked. The two surfaces of this lamella are supported by proteinaceous palisade-like pillar structures (ps) spanning the previous siliceous components. Consequently, the proteinaceous pillars traverse the (previously existing) silica lamella. (H) Higher magnification of the sample shown in (G).

Schulze (1925). Interesting is the observation that in the initial phase of dissolution a continuous organic envelope, the lamellar coating, is exposed which can be stained with Coomassie Brilliant blue. This envelope collapses rapidly and results in the formation of irregular protein aggregates. If the HF-mediated dissolution continues the lamellar zone-derived protein aggregates remain either associated with the remaining spicules, or are liberated into the vicinity.

After extensive dissolution of the silica, the protein aggregates leave the spicule, leaving behind a second organic tubing, the axial barrel, which is embedded in the axial cylinder. This structure is likewise positively stained with Coomassie Brilliant blue. Besides by this dye, this tubing can also be stained with Sirius Red which has been described initially as a specific reagent for the detection of collagen (Junqueira et al., 1979; Taskiran et al., 1999).

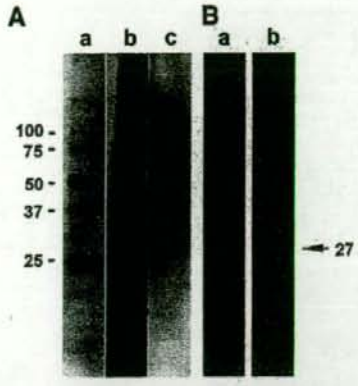

Fig. 8. Analysis of the proteinaceous material released from the lamellar zone. (A) NaDodSO$_4$–PAGE analysis. The matrix protein from the lamellar zone was obtained by limited dissolution of the spicules with HF. Lane b, the almost insoluble protein obtained was (partially) dissolved in PAGE sample buffer and size-separated. Lane c, the sediment was treated with 6 M urea and 10% (v/v) β-mercaptoethanol (30 min at 60 °C), prior to the transfer to the sample buffer. After separation the gel was stained with Coomassie Brilliant blue to visualize the 27-kDa protein. Lane a, protein size markers. (B) Identification of the 27-kDa protein in the extract from the lamellar zone. The protein was released from the lamellae by extraction in a Tris-based lysis buffer, in the absence of HF. The protein sample was reacted with biotinylated E-64 and subjected to NaDodSO$_4$–PAGE and after blot transfer reacted with biotinylated E-64 as described under Section 2. The binding reaction with this reagent was performed, either by direct addition of biotinylated E-64 (lane a) or after a pretreatment with a surplus of unlabeled E-64 (lane b).

It had been proposed that this strong anionic dye stains collagen by reacting with the basic groups present in collagen molecules. Later it was reported that this dye stains also other macromolecules which comprise a triple-helical structure. Interestingly the proteins occupying the axial cylinder, look like twisted rope bundles, which persist in this arrangement even after complete dissolution of the siliceous spicule. Our approaches to identify the nature of the protein(s) forming the bundle have not yet been successful. By NaDodSO$_4$–PAGE we could present evidence that these proteins have a size of around 70 kDa and carry positively and negatively charged side chains (Müller et al., in preparation).

Next, we tried to identify the proteins which are liberated by HF during the dissolution of bio-silica with HF, with main emphasis of the lamellar zone. The silica shell of the spicules had been dissolved in a limited way, so that only the majority of the lamellar zone was dissolved, while the axial cylinder remained intact. The organic material thus obtained appeared as denatured/coagulated protein aggregates, a view which is supported by the fact that the reactions during HF dissolution are exergonic. In addition, it had been reported that HF splits off *O*-glycosidic and phosphate ester bonds in protein (Kröger et al., 1999, 2002). These protein aggregates were analyzed by NaDodSO$_4$–PAGE and found to be only slightly soluble in low-strength buffer. For the solubilization of the proteinaceous aggregates we used high concentration of the chaotropic agent urea (6 M), which disrupts the noncovalent forces; in addition, β-mercaptoethanol (10%) was used to cleave potential disulfide bonds (see e.g., Wood et al., 2006). Applying this procedure we succeeded to demonstrate that the proteinaceous matrix in the lamellar zone is a 27-kDa polypeptide. The size of this protein matches with the mature form of silicatein, found in demosponges (reviewed in Müller et al., 2006a). However, it cannot—at the present time—be ruled out that another species of macromolecules exists within the lamellae, which cannot be

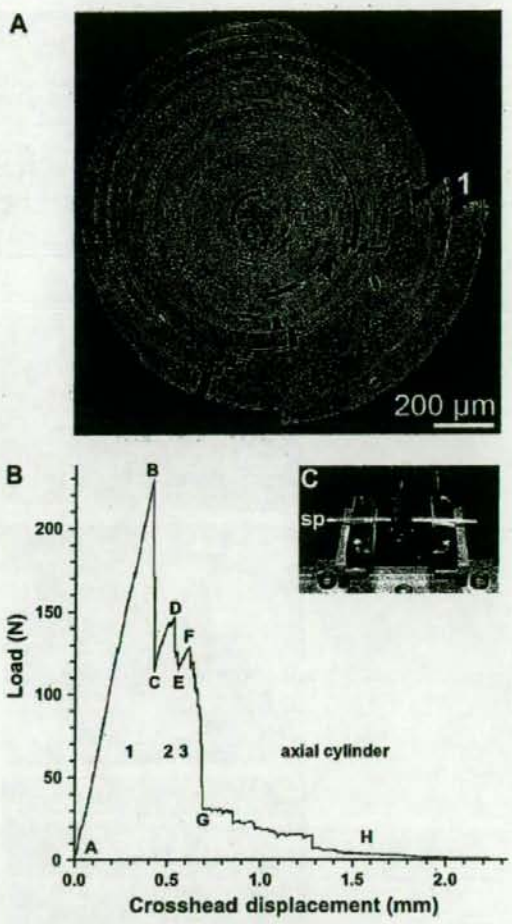

Fig. 9. Force displacement relationship of a giant basal spicule, as measured in a 3-point bending assay. (A) SEM analysis of a partially cracked spicule. Three different crack zones, including several lamellae each, are marked (1–3) in addition to the central axial cylinder (cy). After the third crack the sample was subjected to SEM analysis. (B) Bend test result of the lamellar spicule. The first cracking event comprises the linear increase A–B (elastic response) until the first crack (B) occurs, followed by the deflection to C. Two additional breakage events (2: C–D–E; and 3: E–F–G) are recorded before a random cracking of the different lamellae within the axial cylinder occurs. (C) Three-point bending system; the spicule (sp) is marked.

detected by Coomassie or silver staining. By means of high resolution electron microscopy it could be identified that the protein molecules are arranged within the lamellae as palisade-like pillars; the individual pillars have a diameter of 0.1–0.2 μm and a length of 5–10 μm. Such an organized structure has never been reported before from sponge spicules.

As expected, it was not possible to measure in the HF-extract from the lamellar zone any enzymatic activity (not shown). Therefore, we applied a more gentle extraction procedure, without HF, to obtain the pure 27 kDa protein; no further polypeptide could be detected in this zone. We used the synthetic substrate Z-Phe-Arg-AMC to screen for proteolytic, cathepsin L-like activity. The reason for choosing this substrate bases on the sequence similarity of the silicateins with cathepsins L (Cha et al., 1999). This approach confirmed that the 27-kDa protein from the lamellar zone displays indeed proteolytic activity. This enzymic reaction could be almost completely blocked by the specific cathepsin inhibitor, the natural compound E-64 (Barrett et al., 1982, 2002). Subsequently, we used the biotinylated E-64 successfully for the identification of the 27-kDa protein after size-separation. Intriguing is the apparent size of the molecule, 27-kDa. This value matches with the size of silicatein (see Cha et al., 1999; Müller et al., 2005, 2006a). Therefore, we have some reason to believe that the lamellar zone is composed of one molecule which comprises silicatein-related properties.

In a further series of experiments the mechanical behavior of spicules was studied using the 3-point bending assay. The results obtained, support earlier experiments by Mayer and colleagues (Sarikaya et al., 2001; Mayer 2005; Mayer et al., 2005) and Morse and colleagues (Weaver et al., 2007) and extend them. The process of cracking of spicules was continuously inspected/recorded both by microscopic studies and by the load extension-experiment. Several, consecutively recordable elastic responses of the spicules can be resolved, which are caused by cracks of distinct lamellar piles. These cracks are presumably controlled by the existing (pre)fabricated break structures which are seen across the lamellae. These cracking structures are not restricted to individual lamellae but include stacks of lamellae. The stability of the flexible spicules is even supported by the fact that the crack structures do not occur in the same plane but are apparently randomly dispersed. This conclusion supports the earlier view (Mayer, 2005) that small and thin organic molecules, here the 27-kDa protein, within the inorganic rigid material provide the skeletal structures, e.g. spicules, with the unusual combination of mechanical stability, strength and stiffness. The inner organic-axial barrel, which is composed of rope-like filaments, stabilizes the axial cylinder and provides the spicules with an additional mechanical quality. Here, the spicules are highly flexible, concomitantly with a low mechanical stability.

Based on our studies with the spicules from *Monorhaphis* we obtained no conclusive data that between the individual lamellae of the spicules any organic layer exists. Therefore, we attribute the assumed viscoelastic and/or energy dissipation properties not to a possible organic interphase between the lamellae but to the proteins within them.

In conclusion, the data presented here provide solid evidence that the morphological structure of the hexactinellid *Monorhaphis* giant basal spicule is composed, in addition to the organic axial filament, by two further inorganic/organic layers of hybrid material which are composed of different proteinaceous components. In the lamellar zone the proteins provide the spicules with a high stiffness and a considerable flexibility, while from the core axial barrel the spicules obtain the property to be less tough and highly flexible. The complete understanding and the subsequent utilization/exploitation of the basic strategies of sponges to form the bioorganic/inorganic hybrid compositions analyzed in their spicules, will surely accelerate the development of new composite synthetic biomaterials (summarized in Morse, 2001; Schröder et al., 2007). In addition, it is amazing that those glass-like structures from sponges possess excellent optical transmissibility of visible light, as reported earlier (Aizenberg et al., 2004; Müller et al., 2006b), a property likewise of highest technological interest.

Acknowledgments

This work was supported by grants from the European Commission, the Deutsche Forschungsgemeinschaft, the Bundesministerium für Bildung und Forschung Germany (Project: Center of Excellence *BIOTEC*marin), the National Natural Science Foundation of China (No. 50402023) and the International Human Frontier Science Program.

References

Aizenberg, J., Sundar, V.C., Yablon, A.D., Weaver, J.C., Chen, G., 2004. Biological glass fibers: correlation between optical and structural properties. Proc. Natl. Acad. Sci. USA 101, 3358–3363.

Aizenberg, J., Weaver, J.C., Thanawala, M.S., Sundar, V.C., Morse, D.E., Fratzl, P., 2005. Skeleton of *Euplectella* sp: structural hierarchy from the nanoscale to the macroscale. Science 309, 275–278.

Autumn, K., Majidi, C., Groff, R.E., Dittmore, A., Fearing, R., 2006. Effective elastic modulus of isolated gecko setal arrays. J. Exp. Biol. 209, 3358–3568.

Barrett, A.J., Kembhavi, A.A., Brown, M.A., Kirschke, H., Knight, C.G., Tama, M., Hanada, K., 1982. *L-trans*-Epoxysuccinyl-leucylamido(4-guanidino)butane and its analogues as inhibitors of cysteine proteinases including cathepsins B, H and L. Biochem. J. 201, 189–198.

Barrett, A.J., Rawlings, N.D., Woessner, J.F. (Eds.), 2002. Handbook of Proteolytic Enzymes. Academic Press, Amsterdam, pp. 617–624.

Cha, J.N., Shimizu, K., Zhou, Y., Christianssen, S.C., Chmelka, B.F., Stucky, G.D., Morse, D.E., 1999. Silicatein filaments and subunits from a marine sponge direct the polymerization of silica and silicones *in vitro*. Proc. Natl. Acad. Sci. USA 96, 361–365.

Chimmo, W., 1878. On *Euplectella aspergillum*. Taylor and Francis, London.

Compton, S., Jones, C., 1985. Mechanism of dye response and interference in the Bradford protein assay. Anal. Biochem. 151, 369–374.

Dvorak, J., Delcroix, M., Rossi, A., Vopalensky, V., Pospisek, M., Sedinova, M., Mikes, L., Sajid, M., Sali, A., McKerrow, J.H., Horak, P., Caffrey, C.R., 2005. Multiple cathepsin B isoforms in schistosomula of *Trichobilharzia regenti*: identification, characterisation and putative role in migration and nutrition. Int. J. Parasitol. 35, 895–910.

Eckert, C., Schröder, H.C., Brandt, D., Perovic-Ottstadt, S., Müller, W.E.G., 2006. A histochemical and electron microscopic analysis of the spiculogenesis in the demosponge *Suberites domuncula*. J. Histochem. Cytochem. 54, 1031–1040.

Ehrlich, H., Worch, H., 2007. Collagen, a high matrix in glass sponge flexible spicules of the meter-long *Hyalonema sieboldi*. In: Bäuerlein, E. (Ed.), Handbook of Biomineralization: Vol. 1. The Biology of Biominerals Structure Formation. Wiley-VCH, Weinheim, pp. 23–41.

Hartman, W.D., 1983. Modern Hexactinellida. In: Broadhead, T.W. (Ed.), Sponges and Spongiomorphs, Notes for a Short Course. Department of Geological Sciences, University of Tennessee, Knoxville, Tennessee.

Holmes, R.E., Hagler, H.K., Coletta, C.A., 1987. Thick-section histometry of porous hydroxyapatite implants using backscattered electron imaging. J. Biomed. Mater. Res. 21, 731–738.

Hsu, S.M., Raine, L., Fanger, H., 1981. Use of avidin-biotin-peroxidase complex (ABC) in immunoperoxidase techniques: a comparison between ABC and unlabeled antibody (PAP) procedure. J. Histochem. Cytochem. 29, 577–580.

Junqueira, L.C.U., Bignolas, G., Brentani, R.R., 1979. Picrosirius staining plus polarization microscopy, a specific method for collagen detection in tissue sections. Histochem. J. 11, 447–455.

Krasko, A., Batel, R., Schröder, H.C., Müller, I.M., Müller, W.E.G., 2000. Expression of silicatein and collagen genes in the marine sponge *Suberites domuncula* is controlled by silicate and myotrophin. Eur. J. Biochem. 267, 4878–4887.

Kröger, N., Deutzmann, R., Sumper, M., 1999. Polycationic peptides from diatom biosilica that direct silica nanosphere formation. Science 286, 1129–1132.

Kröger, N., Lorenz, S., Brunner, E., Sumper, M., 2002. Self-assembly of highly phosphorylated silaffins and their function in biosilica morphogenesis. Science 298, 584–586.

Kruse, M., Leys, S.P., Müller, I.M., Müller, W.E.G., 1998. Phylogenetic position of the Hexactinellida within the phylum Porifera based on amino acid sequence of the protein kinase C from *Rhabdocalyptus dawsoni*. J. Mol. Evol. 46, 721–728.

Laemmli, U.K., 1970. Cleavage of structural proteins during the assembly of the head of bacteriophage T4. Nature 227, 680–685.

Levi, C., Barton, J.L., Guillemet, C., Le Bras, E., Lehuede, P., 1989. A remarkably strong natural glassy rod: the anchoring spicule of the *Monorhaphis* sponge. J. Mater. Sci. Lett. 8, 337–339.

Leys, S.P., Mackie, G.O., Reiswig, H.M., 2007. The biology of glass sponges. Adv. Mar. Biol. 52, 1–145.

Mayer, G., Trejo, R., Lara-Curzio, E., Rodriguez, M., Tran, K., Song, H., Ma, W.H., 2005. Lessons for new classes of inorganic/organic composites from the spicules and skeleton of the sea sponge *Euplectella aspergillum*. Mater. Res. Soc. Symp. Proc. 844, Y4.2.1–Y4.2.8.

Mayer, G., 2005. Rigid biological systems as models for synthetic composites. Science 310, 1144–1147.

Morse, D.E., 2001. Biotechnology reveals new routes to synthesis and structural control of silica and polysilsesquioxanes. In: Rappoport, Z., Apeloig, Y. (Eds.), The Chemistry of Organic Silicon Compounds, vol. 3. Wiley, New York, pp. 805–819.

Mort, J.S., 2002. Cathepsin L. In: Barrett, A.J., Rawlings, N.D., Woessner, J.F. (Eds.), Handbook of Poteolytic Enzymes. Academic Press, Amsterdam, pp. 617–624.

Müller, W.E.G., Wiens, M., Adell, T., Gamulin, V., Schröder, H.C., Müller, I.M., 2004. The Bauplan of the Urmetazoa: The basis of the genetic complexity of Metazoa using the siliceous sponges [Porifera] as living fossils. Int. Rev. Cytol. 235, 53–92.

Müller, W.E.G., 2005. Spatial and temporal expression patterns in animals. In: Meyers, R.A. (Ed.), Encyclopedia of Molecular Cell Biology and Molecular Medicine, vol. 13. WILEY-VCH Press, Weinheim, pp. 269–309.

Müller, W.E.G., Rothenberger, M., Boreiko, A., Tremel, W., Reiber, A., Schröder, H.C., 2005. Formation of siliceous spicules in the marine demosponge *Suberites domuncula*. Cell Tissue Res. 321, 285–297.

Müller, W.E.G., Belikov, S.I., Tremel, W., Perry, C.C., Gieskes, W.W.C., Boreiko, A., Schröder, H.C., 2006a. Siliceous spicules in marine demosponges (example *Suberites domuncula*). Micron 37, 107–120.

Müller, W.E.G., Wendt, K., Geppert, C., Wiens, M., Reiber, A., Schröder, H.C., 2006b. Novel photoreception system in sponges? Unique transmission properties of the stalk spicules from the hexactinellid *Hyalonema sieboldi*. Biosens. Bioelectron. 21, 1149–1155.

Müller, W.E.G., Eckert, C., Kropf, K., Wang, X., Schloßmacher, U., Seckert, C., Wolf, S.E., Tremel, W., Schröder, H.C., 2007a. Formation of the giant spicules of the deep sea hexactinellid *Monorhaphis chuni* (Schulze 1904): electron microscopical and biochemical studies. Cell Tissue Res. 329, 363–378.

Müller, W.E.G., Wang, X., Belikov, S.I., Tremel, W., Schloßmacher, U., Natoli, A., Brandt, D., Boreiko, A., Tahir, M.N., Müller, I.M., Schröder, H.C., 2007b. Formation of siliceous spicules in demosponges: example *Suberites domuncula*. In: Bäuerlein, E. (Ed.), Handbook of Biomineralization, The Biology of Biominerals Structure Formation, vol. 1. Wiley-VCH, Weinheim, pp. 59–82.

Müller, W.E.G., Boreiko, A., Wang, X., Belikov, S.I., Wiens, M., Grebenjuk, V.A., Schloßmacher, U., Schröder, H.C., 2007c. Silicateins, the major biosilica forming enzymes present in demosponges: protein analysis and phylogenetic relationship. Gene 395, 62–71.

Ni, G.X., Chiu, K.Y., Lu, W.W., Wang, Y., Zhang, Y.G., Hao, L.B., Li, Z.Y., Lam, W.M., Lu, S.B., Luk, K.D.K., 2006. Strontium-containing hydroxyapatite bioactive bone cement in revision hip arthroplasty. Biomaterials 27, 4348–4355.

Patwardhan, S.V., Clarson, S.J., Perry, C.C., 2005. On the role(s) of additives in bioinspired silicification. Chem. Commun., 1113–1121.

Quian, F., Bajkowski, A.S., Steiner, D.F., Chan, S.J., Frankfater, A., 1989. Expression of five cathepsins in murine melanomas of varying metastatic potential and normal tissues. Cancer Res. 49, 4870–4875.

Radojkovic, D., Kusic, J., 2000. Silver staining of denaturing gradient gel electrophoresis gels. Clin. Chem. 46, 883–884.

Rädlein, E., Frischat, G.H., 1997. Atomic force microscopy as a tool to correlate nanostructure to properties of glasses. J. Non-Cryst. Solids 222, 69–82.

Reiswig, H.M., 2006. Classification and phylogeny of Hexactinellida (Porifera). Can. J. Zool. 84, 195–204.

Sachs, L., 1984. Angewandte Statistik. Springer, Berlin, 242 pp.

Sandford, F., 2003. Physical and chemical analysis of the siliceous skeleton in six sponges of two groups (Demospongiae and Hexactinellida). Microsc. Res. Technol. 62, 336–355.

Sarikaya, M., Fong, H., Sunderland, N., Flinn, B.D., Mayer, G., Mescher, A., Gaino, E., 2001. Biomimetic model of a sponge-spicular optical fiber-mechanical properties and structure. J. Mater. Res. 16, 1420–1428.

Schröder, H.C., Boreiko, A., Korzhev, M., Tahir, M.N., Tremel, W., Eckert, C., Ushijima, H., Müller, I.M., Müller, W.E.G., 2006. Co-expression and functional interaction of silicatein with galectin: matrix-guided formation of siliceous spicules in the marine demosponge *Suberites domuncula*. J. Biol. Chem. 281, 12001–12009.

Schröder, H.C., Brandt, D., Schloßmacher, U., Wang, X., Tahir, M.N., Tremel, W., Belikov, S.I., Müller, W.E.G., 2007. Enzymatic production of biosilica-glass using enzymes from sponges: Basic aspects and application in nanobiotechnology (material sciences and medicine). Naturwissenschaften 94, 339–359.

Schultze, M., 1860. Die Hyalonemen. Adolph Marcus, Bonn.

Schulze, F.E., 1904. Hexactinellida Wissenschaftliche Ergebnisse der Deutschen Tiefsee-Expedition auf dem Dampfer Valdivia 1898–1899. Gustav Fischer Verlag, Stuttgart, pp. 1–266.

Schulze, P., 1925. Zum morphologischen Feinbau der Kieselschwammnadeln. Z. Morphol. Ökolog. Tiere 4, 615–625.

Shimizu, K., Cha, J., Stucky, G.D., Morse, D.E., 1998. Silicatein alpha: cathepsin L-like protein in sponge biosilica. Proc. Natl. Acad. Sci. USA 95, 6234–6238.

Struble, L.J., Stutzman, P.E., 1989. Epoxy impregnation of hardened cement for microstructural characterization. J. Mater. Sci. Lett. 8, 632–634.

Tabachnick, K.R., 2002. Family Monorhaphididae Ijima, 1927. In: Hooper, N.A.V., Soest, R.W.M. (Eds.), Systema Porifera: A Guide to the Classification of Sponges. Kluwer Academic Publishers, New York, pp. 1264–1266.

Tahir, M.N., Théato, P., Müller, W.E.G., Schröder, H.C., Boreiko, A., Faiß, S., Janshoff, A., Huth, J., Tremel, W., 2005. Formation of layered titania and zirconia catalysed by surface-bound silicatein. Chem. Commun. 44, 5533–5535.

Taskiran, D., Taskiran, E., Yercan, H., Kutay, F.Z., 1999. Quantification of total collagen in rabbit tendon by the Sirius Red method. Tr. J. Med. Sci. 29, 7–9.

Walsh, B.J., Thornton, S.C., Penny, R., Breit, S.N., 1992. Microplate reader-based quantitation of collagens. Anal. Biochem. 203, 187–190.

Wang, X., Wang, Y., 2006. An introduction to the study on natural characteristics of sponge spicules and bionic applications. Adv. Earth Sci. 21, 37–42.

Wang, X., Li, J., Qiao, L., Schröder, H.C., Eckert, C., Kropf, K., Müller, W.E.G., 2007. The giant spicules of the deep sea hexactinellidan sponges of the genus *Monorhaphis* (Hexactinellida: Amphidiscosida: Monorhaphididae). Acta Zool. Sin. 53, 557–569.

Weaver, J.C., Aizenberg, J., Fantner, G.E., Kisailus, D., Woesz, A., Allen, P., Fields, K., Porter, M.J., Zok, F.W., Hansma, P.K., Fratzl, P., Morse, D.E., 2007. Hierarchical assembly of the siliceous skeletal lattice of the hexactinellid sponge *Euplectella aspergillum*. J. Struct. Biol. 158, 93–106.

Wiens, M., Belikov, S.I., Kaluzhnaya, O.V., Krasko, A., Schröder, H.C., Perovic-Ottstadt, S., Müller, W.E.G., 2006. Molecular control of serial module formation along the apical–basal axis in the sponge *Lubomirskia baicalensis*: silicateins, mannose-binding lectin and mago nashi. Dev. Genes Evol. 216, 229–242.

Woesz, A., Weaver, J.C., Kazanci, M., Dauphin, Y., Aizenberg, J., Morse, D.E., Fratzl, P., 2006. Micromechanical properties of biological silica in skeletons of deep sea sponges. J. Mater. Res. 21, 2068–2078.

Wood, C.M., Sodngam, S., Nicholson, J.N., Lambert, S.J., Reynolds, C.D., Baldwin, J.P., 2006. The oxidized histone octamer does not form a H3 disulphide bond. Biochim. Biophys. Acta 1764, 1352–1356.

Biofabrication of biosilica-glass by living organisms

Heinz C. Schröder,*[a] Wolfgang Tremel,[b] Xiaohong Wang,[c] Hiroshi Ushijima[d] and Werner E.G. Müller*[a]

Receipt/Acceptance Data **[DO NOT ALTER/DELETE THIS TEXT]**
Publication data **[DO NOT ALTER/DELETE THIS TEXT]**
DOI: 10.1039/b000000x [DO NOT ALTER/DELETE THIS TEXT]

Biosilicification is an evolutionary old and widespread type of biomineralization both in unicellular and multicellular organisms including sponges, diatoms, radiolaria, choanoflagellates, and higher plants. In the last few years combined efforts in molecular biology, cell biology, and inorganic and analytical chemistry allowed first insights in the molecular mechanisms by which these organisms form an astonishing structural variety of siliceous structures not reached by chemical methods. The skeletal elements of two classes of sponges, Demospongiae and Hexactinellida, the siliceous spicules, consist of glassy amorphous silica (biosilica). The demosponges exhibit the unique ability to synthesize biosilica using a novel group of enzymes which have been termed silicateins. Silicateins have been isolated, cloned and sequenced both from marine sponges and freshwater sponges. Sponges also possess a silicase, which mediates the dissolution of amorphous silica. Diatoms, which belong to the Protista, have used an independent strategy to utilize silica for the construction of their skeletal elements. Silica formation in diatoms proceeds nonenzymatically and involves both proteins (silaffins) and long-chain polyamines. The silaffins are post-translationally modified at the ε-amino groups of their lysine residues by addition of methylpropylamine units. Phosphorylation of silaffins at their serine units is necessary for polymerisation of these molecules. The mechanism of deposition of (amorphous) silica in higher plants is less well understood. Silica forming organisms live in an environment that is undersaturated with respect to silicic acid and need to accumulate silicon. cDNAs encoding a silicic acid transporter have been isolated both sponges, diatoms and higher plants. The deduced polypeptide of the demosponge (*Suberites domuncula*) silicic acid transporter is not related to the transporter from the diatom *Cylindrotheca fusiformis*, which also acts as a sodium/silicic acid symporter. A silicon transporter belonging to the aquaporin family of proteins has been identified in higher plants (rice). The proteins/molecules involved in biosilicification, in particular the sponge enzymes, silicatein and silicase, are of potential biotechnological interest for the structure-controlled biofabrication of silica (nano)materials for biosensors, biomedical uses and bio-semiconductors.

[a] *Institut für Physiologische Chemie, Abteilung Angewandte Molekularbiologie, Universität, Duesbergweg 6, D-55099 Mainz, Germany. Fax: +49-6131-3925243; Tel: +49-6131-3925789; E-mail: hschroed@uni-mainz.de*
[b] *Institut für Anorganische Chemie und Analytische Chemie, Universität, Duesbergweg 10-14, D-55099 Mainz, Germany. Fax: +49-6131-3925605; Tel: +49-6131-3925135; E-mail: tremel@uni-mainz.de*
[c] *National Research Center for Geoanalysis, 26 Baiwanzhuang Dajie, CHN-100037 Beijing, China. Fax: +86-10-68999591; Tel: +86-10-68999591; E-mail: wxh0408@hotmail.com*
[d] *Department of Developmental Medical Sciences, Institute of International Health, Graduate School of Medicine, The University of Tokyo, 7-3-1 Hongo, Bunkyo-Ku, Tokyo 113-0033, Japan. Fax: +81-3-5841-3629; Tel: +81-3-5841-3590; E-mail: ushijima@m.u-tokyo.ac.jp*
† Electronic Supplementary Information (ESI) available: [details of any supplementary information available should be included here]. See http://dx.doi.org/10.1039/b000000x/

1 Introduction

Biogenic silica ("biosilica") is formed in many aquatic and terrestric organisms including sponges, diatoms, radiolarians, choanoflagellates, and higher plants.[1-4] The turnover of silicon by silica-forming organisms is enormous. Marine organisms process about 6.7 gigatonnes of silicon every year to build their silica skeletons.[5] Biosilicifying organisms including sponges (approx. 10.000 species) and diatoms (approx. 100.000 species) are able to form a huge variety of biosilica structures which are species-specific and often used as systematic characters for a given species. Biosilicification has also become an inspirational source ("Nature as model") for the development of novel fabrication procedures in nanobiotechnology. Technical production of silica commonly requires high temperatures and pressures, and extremes of pH. Living organisms are, however, able to form silica under ambient conditions, at low temperature and pressure and near-neutral pH.[4] Moreover they produce their silica skeletons with high fidelity. Understanding the mechanism(s) of biosilica formation and identification of the components involved in this process and constituents of biosilica is therefore of high importance for the technological/industrial application of the unique synthetic abilities of silica-forming plants and animals. Silica is, in principle, a mechanical fragile material. However, siliceous organisms use silica as a composite material. Several different classes of biomolecules have been found to be associated with or embedded within the biosilica, including enzyme proteins,[6-12] glycoproteins,[13] polyamines[14] and polyamine-modified peptides.[15-17]

Here we report about the present stage of knowledge on the structure, biochemical composition, and mechanisms of formation of biosilica mainly in sponges, diatoms and higher plants. We focus our attention particularly on biosilicification in sponges because of the enormous (nano)biotechnological potential of the sponge enzymes involved in this process.

2 Silica: chemical aspects

At concentrations above of 1-2 mM and neutral pH, orthosilicic acid [$Si(OH)_4$] undergoes a series of polycondensation reactions, leading to the formation of siloxane (Si-O-Si) bonds.[1,18] Such condensation reactions may involve (i) the reaction between two unionized silicic acid molecules or (ii) the reaction between an ionized and unionized silicic acid molecule. The first process results in the release of water without a change of the pH of the system, while a hydroxyl ion which in non-buffered media increases the pH of the system is liberated in the latter process. The condensation reaction is based on a nucleophilic substitution (S_N2) reaction, resulting in the intermediary formation of a pentacoordinated silicon species.[3]

The condensation process initially results in the formation of dimers which react preferentially with monomers to form trimers and higher oligomers; the latter silicic acid species easily cyclize because of the proximity of the chain ends to form rings of three to six silicon atoms. Oligomer formation renders the silicon atoms more electrophilic (increase in the density of ionized silanol groups), which then become preferential sites for the addition of further silicic acid monomers. The Ostwald ripening process then leads to the growth of larger, less soluble particles by deposition of silicic acid released from smaller, more soluble particels.[3,19] The aggregation of silica particles in solution follows a fractal growth process.[20]

As the pK_a values for the silanol groups decrease with increasing size of the particles (monomeric silicic acid is weakly acidic with a pK_a of 9.8),[18] larger silica particles are ionized and have a negative charge.[3] Therefore, the presence of positively charged molecules or ions is required to neutralize the negative, repulsive surface charge of these silica particles, so that further aggregation can occur. It is well known that the particle size, pore structure, as well as the kinetics of the process of silica formation can be modified by the presence of additives.[18] The condensation process is promoted by the presence of metal cations, which favor silica aggregation by decreasing the negative charge of the silicate particles above pH 7,[21] as well as by cationic polyelectrolytes.[22] Polyamines such as polylysine, polyarginine, and polyallylamine promote the aggregation process by adsorption of silicic acid monomers and oligomers onto the amino groups of these molecules.[23,24]

The polymeric amorphous silica formed consists of a covalently linked network of tetrahedrally coordinated and randomly arranged siloxane centers.[1] It exhibits a variable number of free silanol groups and a variable extent of hydration. Data obtained by infrared spectroscopy indicate that up to one of the four oxygens of the silica tetrahedra exist in the form of a free silanol group;[25] both fully condensed centers (Q_4 sites) and partially condensed centers with one (Q_3), two (Q_2), and three hydroxy groups (Q_1) can be distinguished. The extent of condensation of the silanol groups can be determined also by solid-state ^{29}Si NMR spectroscopy. In addition, the SiO_4 tetrahedra show variable Si–O–Si bond angles and Si–O bond distances.[3]

3 Biosilica structures

3.1 Sponge spicules

Sponges (Porifera) evolved prior to the Cambrian explosion, more than 525 Myr (million years) ago, and are the oldest still existent Metazoa that use silica as a biomineral to form their inorganic skeleton.[26-28] It should be noted that only two classes of sponges, the Demospongiae and the Hexactinellida, have a silica skeleton, while the evolutionary younger third class of sponges, the Calcarea, has spicules made of calcium carbonate.[29] The biosilica produced by sponges, as also the biosilica formed by other organisms, consists of glassy amorphous silica. Small-angle and wide-angle X-ray diffraction analyses of sponge spicules,[30] diatom cell walls[31] and higher plants[32] gave no evidence for the existence of quartz (crystalline silica) in biosilica. Sponge biosilica has a high water content (6 to 13%).[33-35] High resolution magnetic resonance microimaging studies revealed that the water in sponge spicules is largely present in a 'mobile' form.[36] Spicules contain besides silicon and oxygen, small or trace amounts of a number of other elements (mainly Al, Ca, Cl, Cu, Fe, K, Na, S, and Zn;[35,37,38] which may influence the

properties, e.g. the refractive index of biosilica.[39] The silica content of sponges can amount to 75% or more of the dry mass of the animals.[6]

Sponge spicules can be subdivided into megascleres/ macroscleres (e.g. oxeas) and (smaller) microscleres (e.g. spherasters) (Fig. 1).[40] The skeleton of the demosponge *Suberites domuncula* (Fig. 2A) which has been used as a model to study spicule formation (reviewed in Refs 10 and 36) is composed of only two types of megascleres, monactinal tylostyles, which form the main fraction of spicules of this siliceous sponge, and smaller fraction of diactinal oxeas. The tylostyles have one pointed end and one swollen knob (Fig. 1A), whereas the the oxeas have two pointed ends. The spicules of *S. domuncula* can reach lengths of up to 450 µm and diameters of 5 to 7 µm (Fig. 2B). *S. domuncula* is the presently best studied sponge on genetic level (reviewed in Ref. 10).

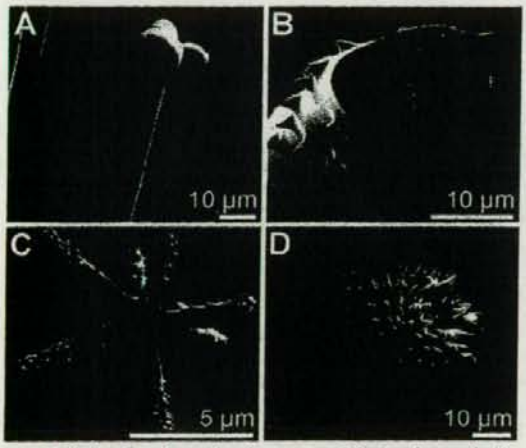

Fig. 1 Spicules from the marine demosponge *Suberites domuncula* (A) and the freshwater demosponge *Lubomirskia baicalensis* (B). Spheraster (C) and sterraster from the marine demosponge *Geodia cydonium* (D). SEM analysis.

In the center of siliceous spicules is a 0.3 to 1.6 µm wide axial canal (Fig. 2C) which harbors an organic (proteinaceous) axial filament (Fig. 2D). The silica is deposited around this axial filament to form concentric ~0.3 to 1 µm thick layers.[38,41] These lamellar silica layers become visible after partial etching of broken spicules (Fig. 2C) and are particularly prominent in spicules from hexactinellid sponges, e.g. *Hyalonema sieboldi* (Fig. 2E,F). Recently we obtained evidence that the silica layers are separated by organic material.[12] Analyses by high-magnification scanning electron microscopy (SEM) and atomic force microscopy (AFM) revealed that the biosilica in spicules has a nanoparticular substructure with a diameter from about 70 nm[42,43] to 100-200 nm.[44]

The formation of sponge spicules is a rather fast process, e.g. in the freshwater sponge *Ephydatia fluviatilis* (spicules length, 100 - 300 µm) they are formed within 40 h.[45,46] The 3D-primmorph culture system of sponges is a very suitable

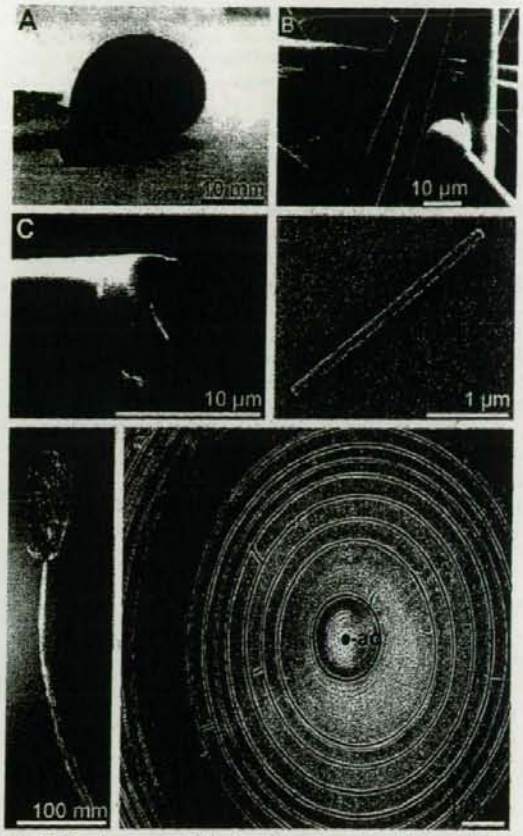

Fig. 2 The demosponge *Suberites domuncula*. (B) Spicules and (C) broken spicule from *S. domuncula* showing the axial canal (ac) (SEM analysis). (D) Axial filament. (E) The hexactinellid sponge *Hyalonema sieboldi*. (F) Cross section (polished) of *H. sieboldi*.

model to study spicule formation.[9] Primmorphs are cell aggregates formed from sponge single cells in the presence of Ca^{2+} ions, that can be obtained from marine and freshwater demosponges (examples: *S. domuncula*[47,48] and *Lubomirskia baicalensis*[49]). Primmorphs contain totipotent archaeocytes which can differentiate to the spicule forming cells, the sclerocytes, in the presence of exogenous silicate.[50] A number of genes involved in biosilica formation and spiculogenesis are upregulated in primmorphs in the presence of silicon, such as those encoding silicatein,[8] silicase,[51] galectin,[12] collagen,[8,52] and noggin, a morphogenetic protein.[53] The optimal concentration of silicon for spicule formation in *S. domuncula* primmorphs is about 60 µM.[8]

3.2 Diatom frustules

Diatoms are unicellular algae living in marine and freshwater habitats; they are divided into two classes, the radially symmetric centrics, and the pennates with an axis of symmetry. Diatoms arose later in evolution than sponges (~260 Ma ago). It is assumed that their occurrence resulted in a strong reduction of the silicon levels of the oceans.

The nanostructured silica patterns of the diatom cell walls (frustules) are species-specific and genetically determined. The frustules are built by silica nanoparticles (50-100 nm) which are surrounded by carbohydrate- and protein-containing organic matrices. They consist of two parts, the epitheca (upper half) and the hypotheca (lower half), which are composed of a valve and several girdle bands (silica strips) (Fig. 3).[54] The valves are usually perforated with pores that show a species specific pattern. The epitheca and the hypotheca overlap in the girdle band region. Both thecae are produced in a specialized vesicle, the silica deposition vesicle (SDV). The SDVs form a weakly acidic compartment (pH 5).[55] Each daughter cell formed during the diatom reproductive cycle has one original frustule and one new valve (Fig. 3). The formation of a new valve is very fast as demonstrated in studies with synchronized cells of the diatom *Navicula salinarum*, using fluorescent stains (PDMPO and rhodamine 123) which are entrapped in the newly formed silica.[56] The architecture and the biosilica composite material of the frustule exhibit remarkable mechanical strength and may provide mechanical protection to the diatom cell.[57] In addition, diatom silica has been proposed to exhibit proton buffering activity.[58]

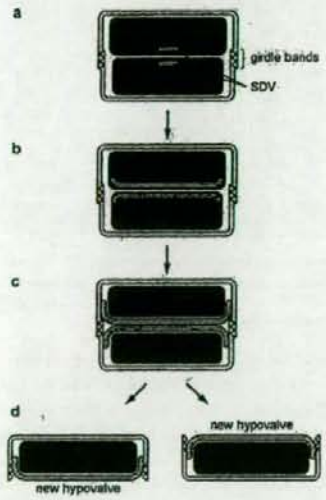

Fig. 3 The diatom reproductive cycle. The two daughter cells are formed inside the parent cell (a). The new hypovalve is formed within the SDV of each daughter cell (b), which is then released by exocytosis (c) before the cells separate (d).

3.3 Biosilica in higher plants

Less is known about biosilica in higher plants than about biosilica in sponges and diatoms. Silicon accumulation and silica deposition vary considerably among different plant species.[59] The silicon content of the shoot dry weight may range from 0.1% to 10% in silicon-accumulating plants such as rice (*Oryza sativa*).[60-63] Silica is deposited on the cell wall of epidermal cells of leaves, stems, and hulls[64,65] where it provides structural support and increases the resistance of plants to diseases, drought and other biotic and abiotic stresses.[60-62,66-69] The silica-cuticle double layer may act as a physical barrier against the penetration of fungi and other pathogens into the epidermal cells.[68] Silicon is furthermore able to induce some enzymatic stress response mechanisms, e.g. the activity of peroxidases, polyphenol oxidases and chitinases.[68,70] Induction of systemic acquired resistance (SAR) in cucumber (*Cucumis sativa*) has been shown to involve the expression of a gene encoding a strongly cationic proline-rich protein (PRP1) with a high amount of lysine and arginine residues; a synthetic peptide derived from this sequence was able to precipitate silica.[71]

3.4 Vertebrates / humans

Silicon is also an essential element in human and many other vertebrates. It is the third most abundant trace element in the human body. The highest silicon concentrations are found in connective tissues such as in bone, skin and blood vessels.[72] Dietary silicon has a critical role in the development of the extracellular matrix (collagen) and bone (hydroxy-apatite) formation.[73-76] Silicon stimulates the formation of type I collagen in human osteoblasts and osteoblast-like cells;[74] it may be involved in the radical-dependent prolyl-hydroxylase pathway during type I collagen formation.[77] Silicon has been identified as a constituent of certain glycosaminoglycans.[78,79] It is absorbed in the gastrointestinal tract in the form of orthosilicic acid.[80]

4 Biosilica formation

4.1 Sponges: Silicatein

The major breakthrough in understanding the molecular mechanism of spicule formation was the discovery of the principle enzyme involved in this process. The axial canal of the spicules harbors an organic filament, the axial filament. This axial filament consists predominantly of a cathepsin L-related enzyme, which was first described by the group of Morse[6,7] and termed silicatein. Their studies (reviewed in Ref. 43) and later studies using biocatalytically active recombinant silicatein[8,11,12] (reviewed in Ref. 81) demonstrated that silica formation in sponges is an enzymatic process. Hence, the mechanism of biosilicification in sponges is distinct from the mechanism of silica formation in diatoms which does not involve any enzyme and is mediated by polyamines[16] and/or polycationic peptides (silaffins).[15,82] Native silicatein isolated from axial filaments as well as the recombinant protein are capable of forming silica from soluble silicon alkoxide precursors in solution.[6,7,8,81]

4.1.1 Silicatein genes/cDNAs

The first silicatein cDNA has been cloned from the marine demosponge *Tethya aurantium*; two isoforms of silicateins (silicatein-α and silicatein-β) have been characterized.[7] Shortly after the genes/cDNAs encoding silicatein-α and silicatein-β have also been cloned from *S. domuncula*[8,10,53,83-85] (Fig. 4) and then also from other marine sponges (*Petrosia ficiformis*),[86] as well as from freshwater sponges.[87-89] Besides the silicatein cDNA from the ubiquitous freshwater sponge *E.*

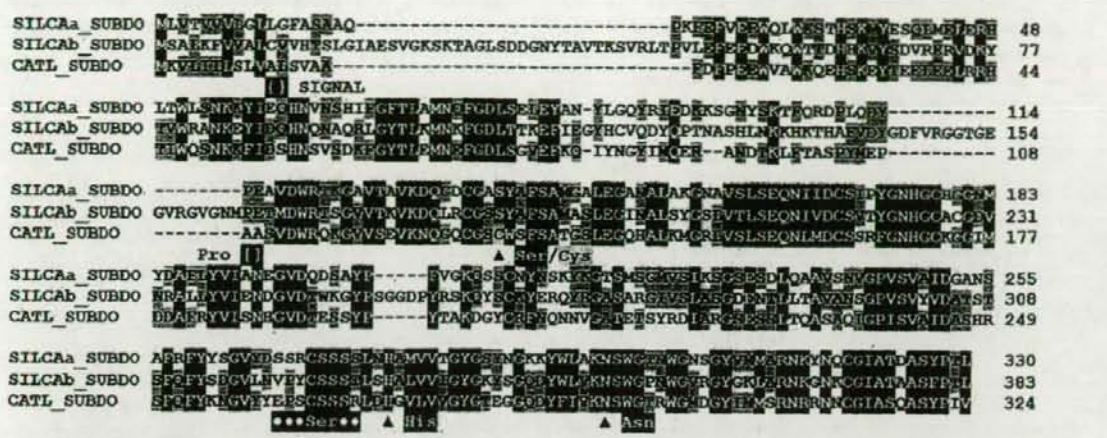

Fig. 4 Sponge silicateins. Alignment of the deduced polypeptide sequences of silicatein-α und silicatein-β from the sponge *S. domuncula* (SILICAa_SUBDO and SILICAb_SUBDO) with cathepsin L from *S. domuncula* (CATL_SUBDO). Residues conserved (similar or related with respect to their physico-chemical properties) in all sequences are shown in white on black and those in at least two sequences in black on gray. The characteristic sites in the sequences are marked; the catalytic triad amino acids, Ser (▲; red) in silicateins [Cys (▲; yellow) in cathepsins] and His (▲; red) and Asn (▲; red), and the processing sites for the conversion of the proenzyme to the mature enzyme (PRO []), the signal peptide (SIGNAL {}), and the serine cluster [•Ser•].

fluviatilis[87] the genes/cDNAs coding for four isoforms of silicatein-α (silicatein a1 to a4) have been identified and characterized in the endemic Baikalian freshwater sponge *L. baicalensis*.[88,89]

The silicateins are related to the cathepsin family of proteases; the highest similarity is shared with cathepsin L (Fig. 4).[6,8,85] The most striking difference between the two groups of enzymes is the presence of a serine residue in the catalytic center of silicateins[6,8] instead of a cysteine residue present in the cathepsins[90] (Fig. 4). The serine residue in silicatein is thought to be essential for the catalytic mechanism of the enzyme (see below). Besides the three amino acids Ser, His and Asn, which form the catalytic center (catalytic triad) of the silicatein, a cluster of hydroxy amino acids (serine cluster) is present (Fig. 4),[6,8] which is located on the surface of the molecule (see Fig. 5A) and may act as template for silica deposition.

The alignment of the deduced amino acid sequence of silicatein-α with the silicatein-β sequence and the cathepsin L sequence from *S. domuncula* is shown in Fig. 4. Prominent sites within the silicatein sequence are the catalytic triad (silicatein-α: Ser aa_{138}, His aa_{277}, and Asn aa_{279}) and the hydroxy amino acid (serine) cluster (aa_{267} to aa_{274}).[6,8] Cathepsins are known to be processed at the C-terminal end of the molecules. The probable processing sites of the primary translation product of silicatein, comprising the signal peptide (ranging from aa_1 to aa_{17}), the propeptide region (aa_{18} to aa_{112}) and the mature chain (aa_{113} to aa_{330}) to the final mature enzyme (aa_{113} to aa_{290}) can be predicted based on the closely related human cathepsin L sequence.[91]

Analyses of the silicatein-α and β genes from *S. domuncula* revealed that they consist of six exons.[92,93] The silicatein-β gene is flanked by an ankyrin repeat gene at one side and by a tumor necrosis factor receptor-associated factor and a protein kinase gene at the other side.[93] All genes of this gene cluster are expressed synchronously in primmorphs following exposure to silicic acid.

In the presumptive 3D structure of silicatein-α obtained by computer modeling using the human cathepsin S as a reference (Swissprot approach), the three amino acids of the catalytic triad, Ser aa_{138}, His aa_{277}, and Asn aa_{279} are present in the active site pocket of the enzyme, while the serine residues of the hydroxyl amino acid cluster are located at the surface of the molecule (Fig. 5A).

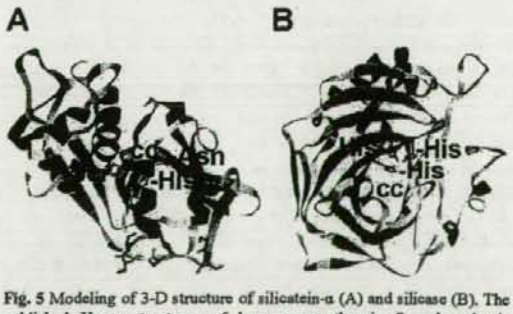

Fig. 5 Modeling of 3-D structure of silicatein-α (A) and silicase (B). The published X-ray structures of human procathepsin S and carbonic anhydrase were used as a reference for modeling the silicatein-α and silicase structure, respectively.[12,109] The catalytic center (cc) of silicatein, comprising the amino acids Ser, His and Asn (yellow) and the localization of the Ser residues (green) of the serine cluster are marked. The silicase model shows the three histidine residues (red), which bind the zinc ion, in the catalytic center of the enzyme. Secondary structure elements are marked in red (α-helices) or blue (β-strands).

The phylogenetic analysis of the silicatein and cathepsins L sequences from marine and freshwater sponges revealed that the silicatein sequences derive from a common ancestor of the cathepsin L sequences (Fig. 6).[11] In addition, the results indicate that the silicateins of the Baikalian endemic sponge

L. baicalensis evolved from the silicateins of the cosmopolitan species *Spongilla lacustris* and *E. fluviatilis* (see also Refs. 94 and 95). The four silicateins of *L. baicalensis* are phylogenetically closely related, suggesting their emergence by gene duplication.[89]

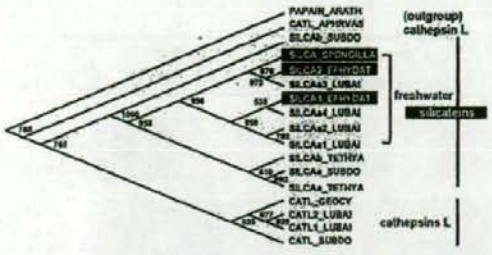

Fig. 6 Phylogenetic relationship of sponge silicateins. Four deduced silicatein sequences of the isoform silicatein-α (α-1, α-2, α-3 and α-4) from *L. baicalensis* (SILICAa1_LUBAI; SILICAa2_LUBAI; SILICAa3_LUBAI; SILICAa4_LUBAI) and the two cathepsin L sequences (CATL1_LUBAI; CATL2_LUBAI) were aligned with silicatein-α from *S. domuncula* (SILICAa_SUBDO) and *T. aurantium* (SILICAa_TETHYA) and with the β-isoenzymes from *S. domuncula* (SILICAb_SUBDO) and *T. aurantium* (SILICAb_TETYHA), as well as with the cathepsin L sequences from *S. domuncula* (CATL_SUBDO), *G. cydonium* (CATL_GEOCY) and *Aphrocallistes vastus* (CATL_APHRVAS) and the related papain-like cysteine peptidase XBCP3 from *Arabidopsis thaliana* (PAPAIN_ARATH) [outgroup]. In addition, the deduced silicateins from the cosmopolitan freshwater sponges *E. fluviatilis* (SILCA1_EPHYDAT and SILCA2_EPHYDAT) and *S. lacustris* (SILCA_SPONGILLA) were included in this analysis. The numbers at the nodes are an indication of the level of confidence for the branches as determined by bootstrap analysis (1000 bootstrap replicates). According to Ref. 95 with modifications.

4.1.2 Catalytic mechanism

Silicatein catalyzes the formation of silica from monomeric silica precursors in solution, such as the synthetic silicon alkoxide, tetraethoxysilane (TEOS), the most commonly used substrate of the enzyme.[7] TEOS is relatively stable when mixed with water at neutral pH, and also used in the industrially applied Stöber process.[96]

Cha *et al.*[7] proposed a two-step mechanism for silicatein-mediated silica formation. Step 1 is the (rate-limiting) hydrolysis of the alkoxide substrate (Fig. 7) and step 2 is the subsequent (poly)condensation reaction of the resulting silanol compounds.

The interaction of the hydroxyl group of the side chain of the serine residue with the imidazole group of the histidine residue in the active site of the enzyme is essential for the catalytic mechanism of the enzyme, as revealed by site-directed mutagenesis experiments.[97] The nucleophilicity of the serine hydroxyl group is thought to be increased by formation of a hydrogen bond to the imidazole nitrogen, thus facilitating the nucleophilic attack (S_N2 type) of the hydroxyl group on the silicon of the alkoxide substrate; a pentavalent intermediate is formed (Fig. 7).[7,97] The transitory covalent linkage between the enzyme and the substrate is then hydrolyzed by water. The reactive silanol molecules generated by hydrolysis subsequently undergo condensation reactions.

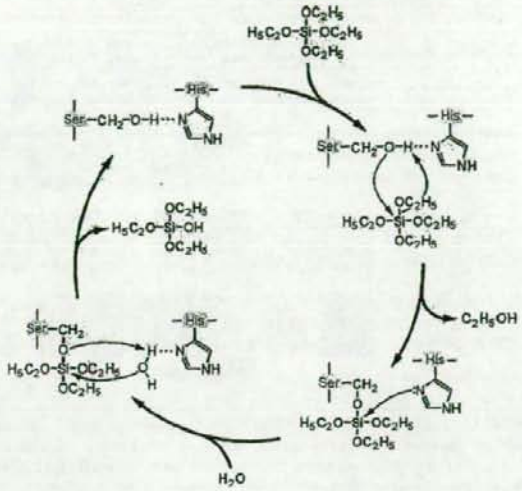

Fig. 7 Proposed mechanism of silicatein reaction. The hydrolysis of the alkoxide substate (rate-limiting step) is shown. According to Ref. 7 with modifications.

It should be noted that silicon alkoxides which are used in *in vitro* assays of silicatein activity are no natural precursor molecules of biosilica formation in sponges. The natural substrate of the enzyme is not yet known. It is known that silicic acid forms complexes with catechols, certain sugars or polyols[98-103] and silicatein has been shown to be closely associated with (sugar-binding) lectins.[12,89] Therefore, silicic acid-sugar complexes might be possible substrates for silicatein. It has been proposed that such complexes are involved in biosilicification in diatoms.[104] It should be noted that silicatein exhibits besides a silica polymerizing activity, a proteolytic (cathepsin-like) activity, which might also be involved in spicule formation.[92]

The mechanism of the condensation reaction (step 2) of the silanol compounds formed in step 1 of silicatein reaction is not known (enzyme/silicatein-mediated vs purely chemical reaction). Molecular simulation experiments indicated that two orthosilicic acid units can be brought together by the rotation of the serine and histidine residues in the catalytic site of the silicatein molecule, through the formation of hydrogen bonds, favoring the the condensation reaction.[105] Model studies of silica formation have been performed using recombinant silicatein and a silicon-catecholate complex (see Scheme 3 in Section 7) that liberates silicic acid in aqueous solution at neutral pH.[106] The results of these studies indicate that silicatein may also control the kinetics of silica polymerization (step 2).

It has also been proposed that the hydroxyl groups of the serine residues are involved in silica deposition by orienting the silicic acid monomers on the protein template.[7] However, the hydroxyl groups of the serin clusters at the surface of the

silicatein molecule cannot *per se* be responsible for the silica deposition at the surface of axial filaments. Silica condensation and deposition have not been observed for cellulose or silk fibroin, although these fibers also have high numbers of hydroxyl groups at their surface.[7]

Silicatein has been reported to catalyze in *in vitro* systems also the formation of organically modified polysiloxanes (silicones) from monomeric precursors.[7] This might be of biotechnological interest (silicon industry).

4.1.3 Maturation of the protein

Silicateins are synthesized as proenzymes which undergo subsequent processing steps to form the mature, active enzymes as demonstrated in protein chemical studies and analyses of the silicatein genes/cDNAs.[9,92] In the first processing step the signal peptide is cleaved from the primary translation product (36.3 kDa) to generate a 34.7-kDa polypeptide; a terminal propeptide is then cleved from the proenzyme to form the mature 23-kDa enzyme.[9] Axial filaments contain only the mature silicatein (23 kDa) which lacks the signal peptide and the propeptide, whereas the proenzyme (34.7 kDa) is the dominant form in the extra-spicule space.[9] Silicatein in the extra-spicule (extracellular) space has been shown to bind to galectin strings forming hollow cylinders along the axis of the growing spicules (see below).[9,10,107] At present it is not known if silicatein is cleaved when associated with spicules.

It is likely that the silicatein proenzyme is enzymatically inactive like the related cathepsin proenzyme.[108] Computer modeling studies revealed that the catalytic pocket in the silicatein proenzyme is blocked by the terminal propeptide sequence.[109] Only after cleavage of the propeptide sequence, the catalytic center becomes accessible to the substrate. This cleavage also occurs during formation of mature (active) cathepsin L from its inactive precursor; it may be mediated by either a second protease or autolysis.[110] The predicted cleavage site of the *S. domuncula* silicatein proenzyme is at aa_{112}/aa_{113} (Gln↓Asp; see Fig. 4).

4.1.4 Post-translational modification

The peptides/proteins involved in silica deposition are extensively modified by post-translational processes both in diatoms and sponges, and these modifications are essential for the function of these molecules. Two-dimensional gel electrophoretic analysis of sponge axial filament protein revealed that silicatein undergoes multiple phosphorylations; five phospho-isoforms with pI values of 5.5, 4.8, 4.6, 4.5, and 4.3 have been identified.[9] Each of these five silicatein phospho-isoforms can be resolved as two or three spots in 2D gels.[11] Electrospray ionization-mass spectrometry analysis of these spots revealed that silicatein also undergoes posttranslational modification by dehydroxylation of tyrosine; the resulting phenylalanine residue is most likely localized on the surface of the molecule as shown by computer modeling of silicatein-α with the human cathepsin S as a reference.[11] The post-translational modifications of the silicatein molecule differ from those of cathepsins which do not form filaments and are only modified by glycosylation and formation of disulfide bonds.[108]

4.1.5 Self-assembly of silicatein filaments

Electron microscopical, small-angle X-ray diffraction (SAXS), protein chemical and computer modelling studies allowed first insights in the mechanism of self-assembly of silicatein monomers to oligomers and long protein filaments. These studies involved the analysis of both isolated axial filaments and soluble, native or recombinant silicatein protein. First SAXS analyses of axial protein filaments revealed evidence for a regular, repeating structure of silicatein units with a periodicity 17.2 nm.[6] However, the filaments used in these studies had been extracted from spicules using a rather harsh procedure (HF treatment) which may cause structural changes of the protein. In a later, more detailed study,[105] the structural organization of spicules from both demosponges and Hexactinellida was investigated. The results from SAXS experiments revealed a very high degree of organization (hexagonal) of the protein units forming the axial filament.[105,111]

Murr and Morse[112] proposed a mechanism for the self-assembly of silicatein monomers to filamentous structures, which proceeds through intermediary formation of a fractal silicatein network. This model assumes that silicatein monomers associate into oligomers by hydrophobic interactions. Silicatein dimers/oligomers can be seen in 1D and 2D gels of axial flament protein, but their occurrence strongly depends on the method used for isolation of the filament.[9,11] The silicatein oligomers are thought to be stabilized by intermolecular disulfide bonds.[112] These oligomers then assemble into fractal intermediates which subsequently form a filament. There is, however, no evidence that in native silicatein sulfhydryl groups are exposed towards the surface of the protein.

It must, however, be taken into account that the method used for isolation of axial filaments may affect the results of studies on silicatein filament formation. HF is known to cause cleavage of O-glycosidic and phosphate ester bonds in proteins.[113] This treatment may therefore result in a loss/change of function of proteins which undergo post-translational modification, as reported for silaffins.[15,17] The availability of *soluble* native or recombinant silicatein protein is absolutely crucial for such studies, aiming to elucidate the mechanism of the self-assembly process of the protein.[9,11]

4.1.6 Localisation of silicatein

Silicatein is present not only in the axial filament but also on the surface of the spicules as shown in immunofluorescence studies and immunogold labeling experiments using anti-silicatein antibodies.[10] The results support the view that growth of spicules occurs through apposition of lamellar silica layers.[9] Detailed electron microscopical analyses highlighted the presence of concentric rings, where silica deposition occurs.[10] These rings are arranged at a distance of 0.2 to 0.5 μm from each other and fuse at a later stage of spicule formation.

4.1.7 Silicatein-associated proteins

Although silicateins are the predominant proteins of the axial filament, a number of further "silicatein-associated" proteins have been identified by analysis of native axial filament

protein isolated by a milder extraction procedure than the harsh HF treatment.[12] These proteins include a 35-kDa protein (galectin-2) and collagen.[12] Furthermore, some minor protein bands are found in SDS-PAGE of spicule extracts, among them a 14-kDa protein (selenoprotein M).[114]

Incubation of primmorphs of *S. domuncula* without or with 60 μM Na-silicate and analysis of the differentially expressed RNA allowed the identification of the cDNA coding for a lectin, galectin-2.[12] Galectin-2 is a galactose-binding lectin, which forms aggregates in the presence of Ca^{2+} ions. It could be demonstrated that silicatein-α molecules bind to these aggregates.[12] In competition experiments the interaction between galectin-2 and silicatein-α was abolished in the presence of a synthetic oligopeptide corresponding to a highly hydrophobic stretch which is present at the *C*-terminus of galectin-2.[12] Electron microscopical and immunogold labeling experiments provided evidence that, together with collagen, galectin-2 serves as a structural matrix for the assembly of silicatein molecules during spicule formation (see Section 8.1).[12]

The expression of two proteins was found to be upregulated after exposure of primmorphs from *S. domuncula* to selenium: selenoprotein M and silicatein-associated protein.[114] The sponge selenoprotein M (14 kDa) is related to other metazoan selenoproteins, whereas the silicatein-associated protein represents a new, sponge-specific protein.[114] The function of the selenium-dependent spicule-associated proteins is not yet known. Immunofluorescence studies revealed that they are present both at the axial filament and the surface of the spicules.[114]

4.2 Diatoms: Silaffins and polyamines

4.2.1 Silaffins

Three groups of proteins have been identified in the cell wall of the marine diatom *Cylindrotheca fusiformis*: (i) the frustulins, (ii) the pleuralins, and (iii) the silaffins (for a review, see Refs 115 and 116).

The EDTA-extractable frustulins are a family calcium-binding glycoproteins with molecular masses of 75 – 200 kDa which form the protective outer coat of the diatom cell wall.[13,117,118]

The pleuralins or hydrogen fluoride extractable proteins (HEPs) are highly acidic molecules with molecular masses of 75 – 200 kDa.[119] They comprise a proline-rich region and several repeats of a PSCD domain. The pleuralins do not induce silica formation. The 200-kDa HF-extractable protein HEP200 from *C. fusiformis* has been characterized.[119] HEP200 is located within the girdle band region of the diatom cell wall where the epitheca overlaps the hypotheca (Fig. 3).[119]

The silaffins have low molecular masses of 4 - 17 kDa and can also be extracted from the diatom cell wall using anhydrous HF.[17] Three polypeptides, silaffin-1A, silaffin-1B and silaffin-2, have been identified in *C. fusiformis*.[15] Silaffin-1A comprises two peptides, silaffin-$1A_1$ and -$1A_2$, which are very similar and, like silaffin-1B, contain lysine groups which are modified (ε-N,N-dimethyllysine and δ-hydroxy-ε-N,N,N-trimethyllysine).[120] A silaffin gene has been cloned and sequenced.[15,82] The deduced polypeptide comprises seven lysine and arginine clusters containing repeat units (R1-R7). Silaffin-1B derives from R1, while silaffin-$1A_1$ and silaffin-$1A_2$ originate from R2-R7.

Using a milder extraction procedure (use of NH_4F/HF) native silaffins, termed natSil could be isolated from *C. fusiformis*.[17] In the native silaffins both lysine and serine residues were found to be modified. The ε-amino groups of the lysine residues in natSil-$1A_1$ (molecular mass, 6.5 kDa) are modified by forming ε-N-dimethyl-lysine or ε-N,N,N-trimethyl-δ-hydroxy-lysine residues or they carry a long-chain polyamine consisting of about 5 to 10 N-methylpropylamine units.[15,17,82] The serine residues and the hydroxyl group on the modified lysine are phosphorylated.[17] Thus natSil-$1A_1$ carries a high number of both positive and negative charges. The structure of natSil-$1A_1$ is shown in Scheme 1.

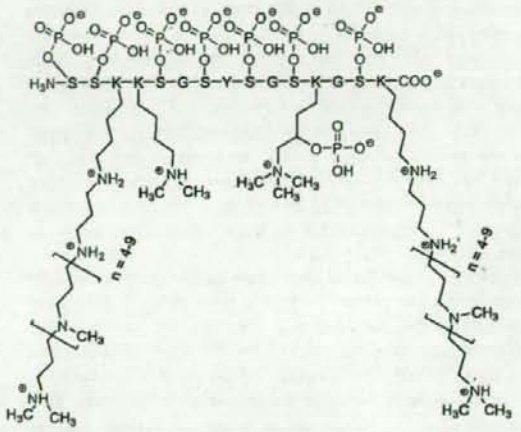

Scheme 1 Schematic structure of silaffin 1A (natSil-1A) from *C. fusiformis*. The structures of the side chains of the modified lysine (K) residues and the phosphorylated serine (S) residues are shown. According to Ref. 17 with modifications.

Mixtures of silaffins 1A, 1B and 2 from *C. fusiformis* are able to cause silica precipitation from a solution of silicic acid forming nanoparticles with diameters of less than 50 nm.[15] Larger particles of 500-700 nm in diameter are obtained in the presence of purified silaffin-$1A_1$ and silaffin-$1A_2$.[82] The polypeptides are occluded in the precipitated silica. The size of the silica nanospheres formed *in vitro* by the purified proteins is larger than the size in diatoms where silica particles of 10 to 100 nm in diameter are found. Silaffins isolated by the harsh HF procedure require addition of phosphate to the incubation mixture for silica precipitation.[15,16,82] Native, phosphorylated silaffins (natSil-1A) are able to precipitate silica also in the absence of additional phosphate.[17] It is assumed that a template for silica precipitation is formed through self-assembly of the zwitterionic silaffin molecules.[17]

In addition to the proteins described above, a homologue of ubiquitin (8.5 kDa) which might be involved in silica biomineralization has been identified by screening of